Planetary and Space Science 60 (2012) 86–92

Contents lists available at ScienceDirect

Planetary and Space Science

journal homepage: www.elsevier.com/locate/pss

Dissipation of Titan's north polar cloud at northern spring equinox

Stéphane Le Mouélic [a,*], Pascal Rannou [b], Sébastien Rodriguez [c], Christophe Sotin [a,d], Caitlin A. Griffith [e], Lucille Le Corre [a], Jason W. Barnes [f], Robert H. Brown [e], Kevin H. Baines [d], Bonnie J. Buratti [d], Roger N. Clark [g], Philip D. Nicholson [h], Gabriel Tobie [a]

[a] Laboratoire de Planétologie et Géodynamique, CNRS, UMR6112, université de Nantes, 2 rue de la Houssinière, BP92208, 44322 Nantes cedex 3, France
[b] GSMA, Université de Reims, France
[c] Laboratoire AIM, CEA, Gif/Yvette, France
[d] JPL, Pasadena, USA
[e] Lunar and Planetary Lab and Steward Observatory, University of Arizona, Tucson, USA
[f] Department of Physics, University of Idaho, Engineering–Physics Building, Moscow, ID 83844, USA
[g] USGS, Denver, USA
[h] Cornell University, USA

ARTICLE INFO

Article history:
Received 31 August 2010
Received in revised form
28 March 2011
Accepted 7 April 2011
Available online 19 April 2011

Keywords:
Titan
Cloud
Meteorology
Cassini
VIMS

ABSTRACT

Saturn's Moon Titan has a thick atmosphere with a meteorological cycle. We report on the evolution of the giant cloud system covering its north pole using observations acquired by the Visual and Infrared Mapping Spectrometer onboard the Cassini spacecraft. A radiative transfer model in spherical geometry shows that the clouds are found at an altitude between 30 and 65 km. We also show that the polar cloud system vanished progressively as Titan approached equinox in August 2009, revealing at optical wavelengths the underlying sea known as Kraken Mare. This decrease of activity suggests that the north-polar downwelling has begun to shut off. Such a scenario is compared with the Titan global circulation model of Rannou et al. (2006), which predicts a decrease of cloud coverage in northern latitudes at the same period of time.

1. Introduction

Besides Earth, Titan is the only place in the Solar System to be veiled by a thick atmosphere, with condensable species that form clouds and possibly rain (Tomasko et al., 2005; Turtle et al., 2011). This atmosphere, with a surface pressure close to the terrestrial value, contains primarily nitrogen and a few percent of methane, up to 5% at the surface (Niemann et al., 2005). The dissociation of methane and nitrogen by ultraviolet sunlight and energetic electrons from Saturn's magnetosphere produces hydrocarbons and nitriles, which react to create more complex molecules as the origin of a photochemical haze. Titan's north polar latitudes, where the temperatures are the coldest during the winter season (2002–2009), provide a cold trap for several species produced by both chemistry and atmospheric transport processes, with strong winds blowing around the pole (Flasar et al., 2005).

Clouds on Titan have been remotely observed by Earth-based telescopes since 1995 (Griffith et al., 1998; Brown et al., 2002; Roe et al., 2005; Schaller et al., 2006) and by the instruments onboard the Cassini spacecraft (Porco et al., 2005; Griffith et al., 2005, 2006; Turtle et al., 2009; Rodriguez et al., 2009; Turtle et al., 2011). They regularly appear, primarily as convective methane clouds, on the south pole and on a belt located at ~40°S. A few isolated and sporadic clouds, convective in origin, have also been observed in tropical regions (Griffith et al., 2009; Schaller et al., 2009), and at northern latitudes, where they have been interpreted as streaks resulting from lake evaporation and polar windshear (Brown et al., 2009). In addition to the discrete and optically thick methane clouds, a vast optically thin cloud was detected in December 2004, August and September 2005 at 50°N latitude and all observable longitudes, and extended to at least the terminator at 68° latitude (Griffith et al., 2006). This cloud was hypothesized, based on its altitude, mass and particle size to be an ethane cloud that capped the north pole, resulting from the winter downward mixing of photochemically produced species in the upper atmosphere (Griffith et al., 2006; Rannou et al., 2006). Ethane being the most abundant available species to condense, this leads to the preferential condensation, sedimentation and possibly surface accumulation of ethane ice. Yet, as the north pole region was not illuminated, the cloud was not fully visible at the

* Corresponding author. Tel.: +33 2 51 12 54 65; fax: +33 2 51 12 52 68.
E-mail address: stephane.lemouelic@univ-nantes.fr (S. Le Mouélic).

0032-0633/$ - see front matter © 2011 Elsevier Ltd. All rights reserved.
doi:10.1016/j.pss.2011.04.006

time of this detection. Cloud spectral signatures were also systematically detected at latitudes higher than 50°N between July 2004 and December 2007 (Rodriguez et al., 2009), but the detailed structure was not investigated.

Here we report spectral images of the north polar cloud, as it extends all the way to the north pole, with VIMS (Visual and Infrared Mapping Spectrometer) measurements onboard the Cassini spacecraft. In Section 2, we describe the first resolved VIMS data of the north polar regions, which were acquired during the T22 flyby in December 2006, and we show different color composites emphasizing the cloud morphology. The temporal evolution of the cloud is then discussed in Section 3 using the images, which have been acquired with the highest spatial resolution and the most favorable observing geometry through June 2009. In Section 4, the data are finally analyzed with a radiative transfer model to study the cloud's opacity and altitude during the years that extend from 2006 to 2009, and the temporal evolution is compared to the predictions of the Titan global climate model (GCM) of Rannou et al. (2006).

2. Observations of the illuminated north pole with VIMS

The VIMS imaging spectrometer acquires hyperspectral images using a detector of 64 × 64 pixels in the spatial dimension. For each pixel of an image, a 352-channels spectrum is acquired in the range from 0.3 to 5.1 μm (Brown et al., 2004). Since the Cassini arrival in 2004, Titan has been observed once a month on average, with 70 flybys performed during the 6 years of the nominal and extended missions (Barnes et al., 2009). The trade-off between different instruments' time allocation and the poor illumination condition as Titan experienced winter in the north hemisphere in the 2004–2009 period prevented the mapping of northern regions on a regular basis. We therefore focused our analysis on the images that have been acquired with the highest spatial resolution and the most favorable observing conditions only. The main characteristics of these observations are summarized in Table 1.

The first good opportunity to observe the half-lit north pole occurred on December 28, 2006, during the flyby labeled T22 (Fig. 1). The T22 data (Table 1 and Fig. 1) were acquired from a distance of 90,000 km with a spatial resolution of 45 km/pixel. The half-lit north pole appeared covered by a huge cloud system, confirming previous expectations (Griffith et al., 2006), and the cloud morphology was revealed for the first time. Fig. 1a shows the integrated flux between 4.90 and 5.09 μm (hereafter called the 5 μm window). Fig. 1b displays a RGB color composite (R=2.78 μm, G=3.26 μm and B=3.33 μm) revealing three different layers in the atmosphere, well above the cloud itself. It shows in particular the fluorescence of methane (in green) in the upper atmospheric layers. Fig. 1c displays a RGB color composite with red=5 μm, green=2.78 μm and blue=2.03 μm. The windows at 5 and 2.78 μm are particularly sensitive to cloud features (Rodriguez et al., 2009). Unlike Titan's southern clouds, this northern cloud is diffusely spread over a very large area. We see in Fig. 1c that the clouds extend from 64°N in latitude up to the north pole, and are surrounded by a diffuse hood down to latitudes of 55°N. It is interesting to note that lakes as imaged by the RADAR in SAR mode are also found in these latitudes (Stofan et al., 2007; Hayes et al., 2008).

3. Evolution of the north polar cloud with time

The evolution of the north polar cloud with time is revealed in Fig. 2, which displays the most resolved VIMS global views of the

Table 1
Characteristics of the VIMS data cubes used in this study. A line mode, corresponding to the acquisition of a series of 1 × 64 lines, was used during the T22 and T42 flybys. Series of 4 × 64 and 6 × 64 cubes were used for the T51 and T54 flybys.

Flyby name and date	Cube label	Exposure time (ms)	Phase angle (°)	Spatial resolution (km pixel^{-1})	Coordinates of haze (h) and cloud pixels used for the radiative transfer
T22	S26/TEMPMAP001/CM_1545974724_1 to	80	113	45	(76,14)h; (75,15); (76, 15); (77,15)
2006 Dec 28	CM_1545983419_1				
T23	S27/MIDIRLIMB002/CM_1547344493	160	110	71	(12, 33)h; (14,32); (14,33); (14,34)
2007 Jan 13					
T29	S29/MEDRES001/CM_1556335256	110	37	55	(33,14)h; (32,15);(29,28); (30,28);(31,28)
2007 April 27					
T42	S39/FIRNADCMP001/CM_1585163262_1 to	280	73	45	(16,66)h; (15, 65);(14,66); (15,66)
2008 Mar 26	CM_1585166504_1				
T43	S40/LIMB001/CM_1589299348_1	160	81	58	(41, 14) h; (42, 14) (43,14); (42, 15)
2008 May 12					
T44	S40/GLOBMAP901/CM_1590679103	95	88	65	(26, 28)h; (26, 27); (25,28); (24,28);(26, 29)
2008 May 28					
T51	S49/FIRNADCMP002/CM_1616829602_1 to	320	106	30	(187,003)h; (182,005) (183,06); (185,007)
2009 Mar 27	CM_1616839616_1				
T52	S49/Medresdrk001/CM_1617472236	120	108	83	(07,23) h; (6,22); (7, 22); (5,23)
2009 Apr 03					
T54	S50/FIRNADCMP002/CM_1620240489_1 to	240	119	45	(17,20) h; (16,19); (17, 19); (16, 20); (24,29)h; (25,29); (25,30); (24,31)
2009 May 05	CM_1620247876_1				
T56	S50/MEDRESDRK001/CM_1622988062_1	320	129	65	(26,19)h; (25,18); (26,18); (24,19);
2009 June 06					

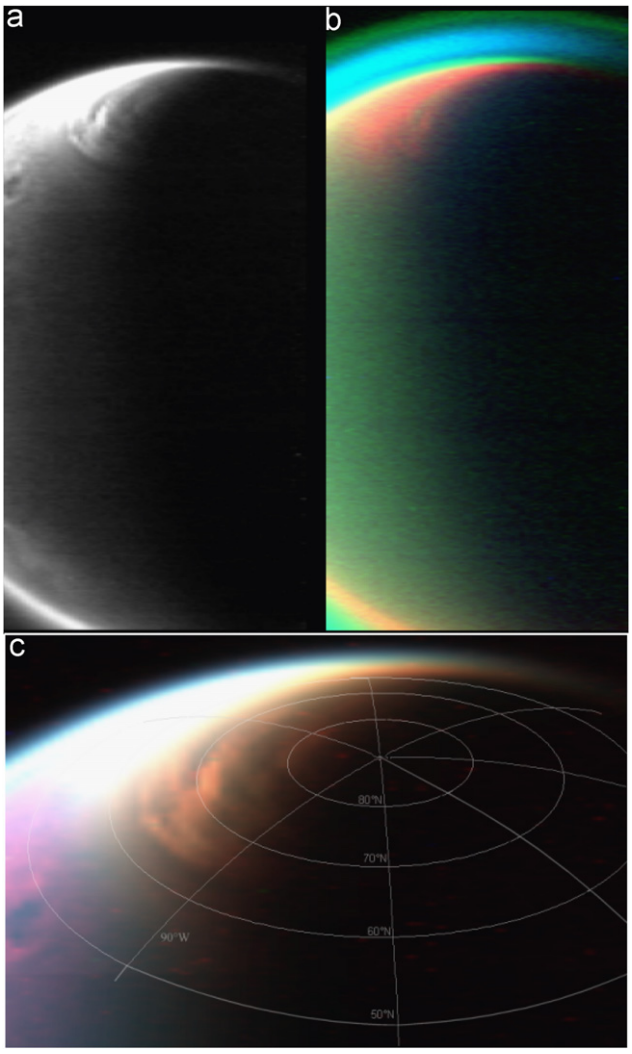

Fig. 1. Imaging of the north polar cloud with VIMS data acquired in 22 December 2006. (a) average of 14 channels in the 5 μm spectral window. (b) color composite with R=2.78 μm, G=3.26 μm, B=3.33 μm showing different layers in the atmosphere. The methane fluorescence at 3.26 μm appears in green in the uppermost layers. (c) color composite with red=5 μm, green=2.78 μm, blue=2.03 μm, with the coordinates grid showing latitudes every 10° and longitudes every 45°. The clouds extend from 64°N in latitude up to the north pole, and are surrounded by a diffuse hood down to latitudes of 55°N.

north pole acquired between T22 (22 December 2006) and T56 (6 June 2009) in raw geometry and using an orthographic projection centered on the north pole. The northern cloud system was observed by VIMS two weeks after the T22 observation, on January 13, 2007, with a lower spatial resolution (flyby T23). It is still present in an image taken at T29 on April 27, 2007, and one year later in the two VIMS images acquired on 25 March 2008 and 12 May 2008 (T42, T43). A similar structure was observed during T44 on 28 May 2008, with less elongated and less bright clouds. It should be noted that starting from the T42 image, it seems that the north cloud begins to break up in some places, leaving a zone that appears much less opaque than the surroundings at ~70°N. The T51 and T52 images in March and April 2009 confirm this observation. The north cloud is at this time much less widespread than in previous observations, showing a very diffuse cloud pattern, and revealing the underlying Kraken Mare (red arrows in Fig. 2). Kraken Mare corresponds to the largest exposure of liquids in the northern regions. It is therefore interesting to note that, from this T52 observation, it will be directly possible to investigate the composition of liquids in the northern regions using infrared spectroscopy. This falls beyond the scope of our paper focused on clouds. The T54 observation acquired later in May 2009 confirms the diminution of cloud activity and shows again Kraken Mare through the diffuse cloud cover. Finally, the T56 observation on 6 June 2009 also displays a much smaller and more confined cloud system, starting at latitudes of ~64°N.

The polar region is surrounded by a ring of a thicker haze and mist mixture whose opacity smoothly rises from about 55°N to the edge of the polar cloud at 62°N. This is well seen in the image taken during T22 (Fig. 1) and was analyzed by Rannou et al. (2010). When the polar cloud breaks up, we can observe an annular zone of brightness. The outer limit of the ring is due to the gradual increase in opacity from about 55°N to 62°N. The inner limit is produced by the break-up of the polar cloud, which seems to leave a zone clear of haze and cloud near the pole. This clear zone appears readily on the images taken during T51 and T54. The ring appears brighter in infrared methane windows because it corresponds to a larger amount of scatterers. It would also appear darker at wavelengths smaller than about 0.62 μm because it contributes in obscuring the bright Rayleigh scattering of the atmosphere. It should be noted that a similar collar was encircling the north polar region, at latitudes around 65°N, during the Voyager flyby in 1981 almost one Titan year earlier (e.g., Sromovsky et al., 1981). A collar was also observed around the south polar region in the winter season in 1999 and 2000 (Roe et al., 2002), but around 70°S or 75°S.

Considering the molar composition of Titan's atmosphere, and the triple point temperatures for methane and ethane (Lavvas et al., 2008), both methane and ethane clouds could form and coexist in the north polar region. Indeed, temperatures in the north polar areas at the time of our observations are found to drop below the freezing point of ethane (Jennings et al., 2009). The small localized clouds, which outbursts near the pole at T51, T54 and T56 might therefore correspond to methane clouds embedded within more diffuse ethane clouds. We tried to discriminate between ethane and methane clouds using a comparison of the 2.8 and 5 μm windows, respectively, in particular in images where both types of clouds seemed to be present. However, no systematic behavior between the two types of clouds did show up in this analysis, which would have allowed their discrimination. The geometry of observation is here the primary responsible for the brightness variations, more than the intrinsic composition and/or the radius of the particles. We also looked for spectral signatures within the broad 5 μm window to discriminate ethane from methane, but again, no diagnostic absorption band was observed in the signal. Finally, the ethane cloud appears readily in the 5 μm image shown in Fig. 1a, which indicates that the particle size is probably bigger than the 3 μm originally derived from the analysis of the 2006 VIMS images of the edge of the cloud in Griffith et al. (2006). The particle size and the link with the actual flux at 5 μm is therefore not an unambiguous way to discriminate between condensed ethane and methane. As liquid ethane and methane have very similar optical constants in the near-infrared, their discrimination is not straightforward, even with the use of high fidelity radiative transfer models. Our conclusion is that the discrimination of the two species of clouds, apart from morphological considerations (widespread diffuse cloud versus more localized, convective in origin clouds) cannot be done unambiguously. We therefore decided to leave the investigation of the composition of the clouds to further studies and to concentrate in the paper on the distribution and temporal evolution of these clouds.

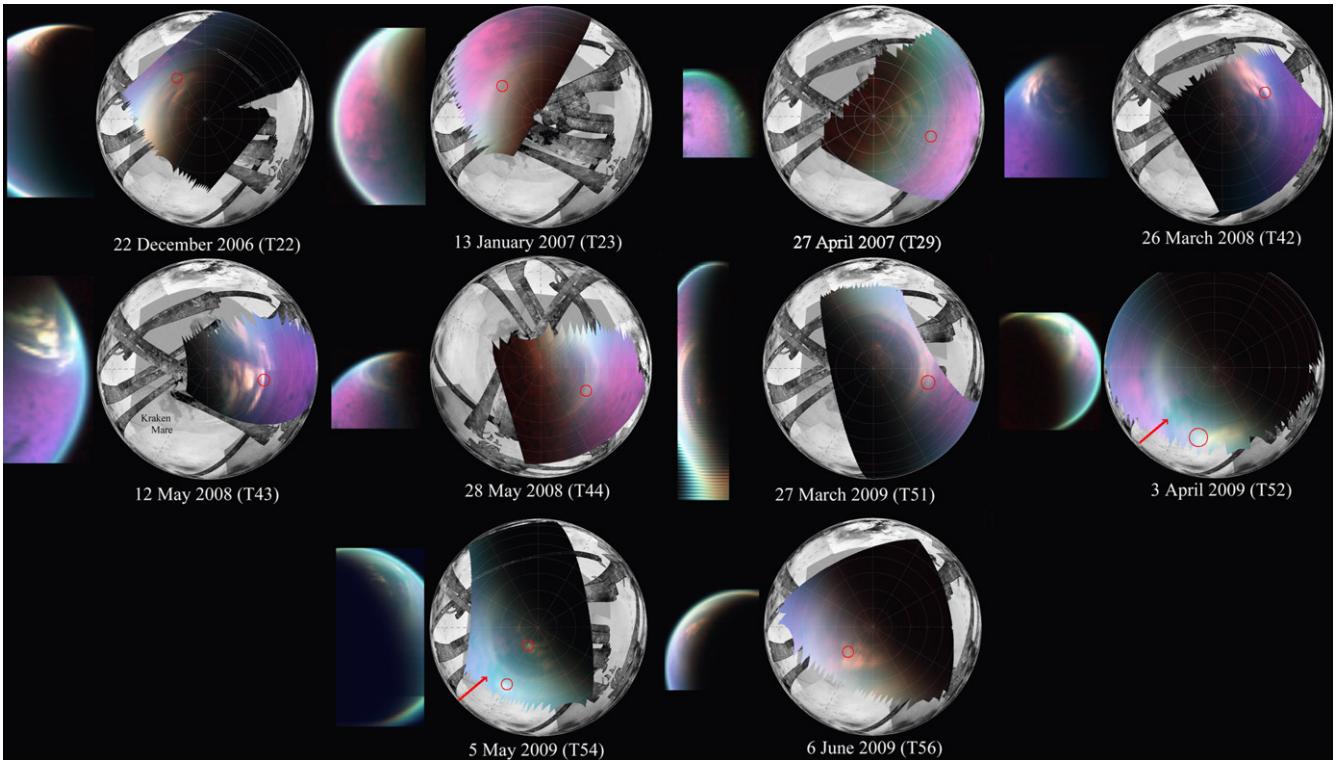

Fig. 2. Selection of the highest-resolution VIMS images of the northern cloud (Red=5.0 μm, Green=2.8 μm, Blue=2.03 μm) between 22 December 2006 and 6 June 2009. Each pair of images shows the north polar region of Titan in raw acquisition geometry (left) and reprojected in north polar orthographic projection (right), with a grid of 10° in latitudes and 30° in longitude (90°E is down). An ISS and RADAR mosaic is used as background. The red circles correspond to the locations of the points used for the radiative transfer modeling. The massive cloud is much less dense and widespread in the last observations (particularly at T51, T52 and T54), revealing the underlying Kraken Mare (red arrows), and an internal annular area centered at ~70°N which appears much less opaque than the surroundings.

4. Determination of the altitude of the cloud using a spectral analysis

We have characterized the altitudes and opacities of these clouds by modeling their spectra. The atmosphere model is similar to the one published in Rannou et al. (2010). We assume, following Tomasko et al. (2008), that aerosols are fractal aggregates of 3000 monomers of 0.05 μm, distributed with vertical profiles scaled from the GCM Database (Rannou et al., 2005). Aerosol optical constants come from Rannou et al. (2010). Below 80 km, we assume that the scatterers are a mixture of aerosols and condensation droplets of 3 μm. The relative proportion of each type of particle is set in order to fit the spectral opacity observed by DISR between 30 and 80 km (Tomasko et al., 2008). The gaseous methane absorptions are taken from the band model published by Irwin et al. (2005, 2006) and modified by Karkoschka and Tomasko (2010). The gaseous methane mixing ratio and temperature profiles used to compute methane absorptions come from Niemann et al. (2005) and Fulchignoni et al. (2005), respectively. Notably, gaseous methane absorption does not depend significantly on the temperature profile, so we can use this profile at whatever latitude we consider. To deal with VIMS data, we use an exponential sum fitting technique that allows the use of weighted calculations with four different values for each VIMS channel. Once the atmosphere properties are set, we use the pseudo-spherical radiative transfer code SPSDISORT (Mayer and Kylling, 2005). As the radiative transfer modeling is very computer intensive, we have selected up to four cloud pixels for each observation. Separate fits were performed to different regions within each red circle in Fig. 2.

To retrieve cloud properties, we use a goodness test to compare the modeled spectra with the observed spectra in the 1.27–1.42 μm region. We do not use the 1.6 μm window to avoid the VIMS filter gap at 1.6 μm (Brown et al., 2004). We do not use the 2.0 μm either, because the shape of the 2.0 μm window is not correctly modeled, probably due to the pressure-induced absorption, which is not correctly represented. Finally, the 2.8 μm window is also extremely complex and many components are still not correctly known. The haze optical constant varies rapidly in this window, CH_3D and C_2H_2 absorbs light while their abundances are poorly known in the low stratosphere, and finally an absorption source is lacking at 2.74 μm (Rannou et al., 2010). These uncertainties therefore make this 2.8 μm window unsuitable for an accurate analysis. To retrieve the cloud properties, we compare the spectrum of a pixel on the cloud with the spectrum of a pixel taken near, but outside the cloud (Fig. 3 and Table 1). The latter spectrum will be a reference haze spectrum, and the cloud pixel will differ from this reference because of the effect of the cloud, and to a lesser extent, due to geometry. For each case, the first step is to find an atmosphere model to fit the reference haze spectrum. To drive our analysis, we assume that clouds are uniform in extinction, with a vertical thickness of $\Delta Z=20$ km independent of the cloud top. This thickness value is derived from the results of the IPSL-GCM (Rannou et al., 2006) updated with new values for the humidity at the surface and the saturation pressure level of N_2–CH_4 mixtures. The two free parameters of the model are the top altitude of the cloud, Z_t and the total opacity of the clouds, τ_c. We have performed several tests that have shown that neither the top altitude nor the total opacity are deeply modified by the choice of the cloud thickness. The sensitivity of the outgoing intensity to the surface albedo is negligible in the considered window, due to the geometry of our observations. To do the analysis, we use an arbitrary value of 0.1 for all wavelengths. We then model the intensity in the cloud pixel using the

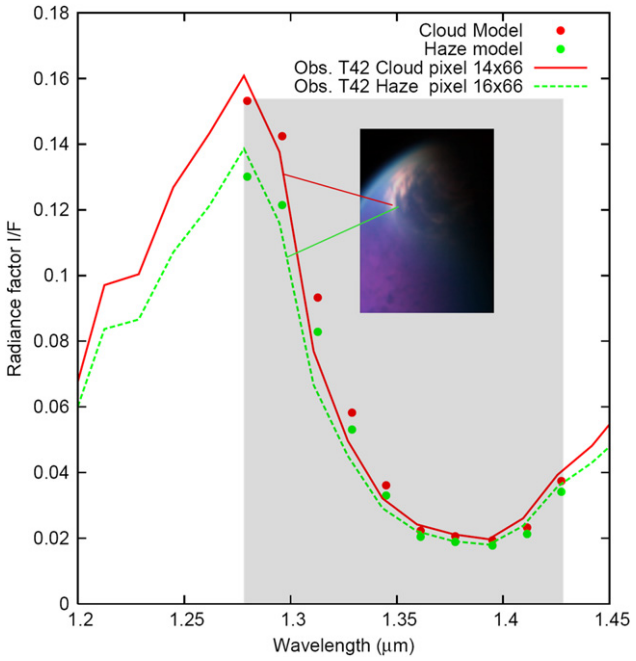

Fig. 3. Comparison between the cloud and haze spectra extracted from the T42 pixels shown in the inset and corresponding results of the radiative transfer model. The fit is computed using the 1.27–1.42 μm wavelength range (see text).

same atmospheric properties as for the reference haze pixel, changing the observing geometry and adding the cloud properties (Z_t,τ_c). Instead of fitting the spectrum of a cloud pixel, which also depends on the quality of the fit for the haze pixel, we fit the difference between the cloud pixel and the reference haze pixel ($\Delta I/F = I/F_{cloud} - I/F_{haze}$). The altitude of the cloud in the model is therefore essentially controlled by the wavelength where the intensity of the cloud pixel departs from the intensity of the haze pixel. An example of this process is shown in Fig. 3 (colored dots) for the T42 observation. The parameters are free in the ranges $18\ \text{km} < Z_t < 70\ \text{km}$ and $0 < \tau_c < 10$. The goodness function is defined as

$$\chi^2 = (N-2)^{-1} \Sigma (\Delta I/F_{OBS} - \Delta I/F_{MODEL})^2 / (I/F_{OBS})$$

where N is the number of VIMS channels used for the fit. With this approach, we obtain maps of χ^2 that indicate the best fit and provide an estimate for the error bars.

We find that the cloud tops always fall in the same altitude range, between 30 and 65 km, with an uncertainty of 15 km in the most favorable cases (Fig. 4a). The modeling analysis did not allow to derive the altitude for the flybys T44, T52 and T56, probably due to a combined effect of the low spatial resolution and of the progressive decrease of the cloud thickness. The derived range of altitudes falls in a region where both methane and ethane clouds can chemically and dynamically occur. It can therefore not be used to unambiguously discriminate between

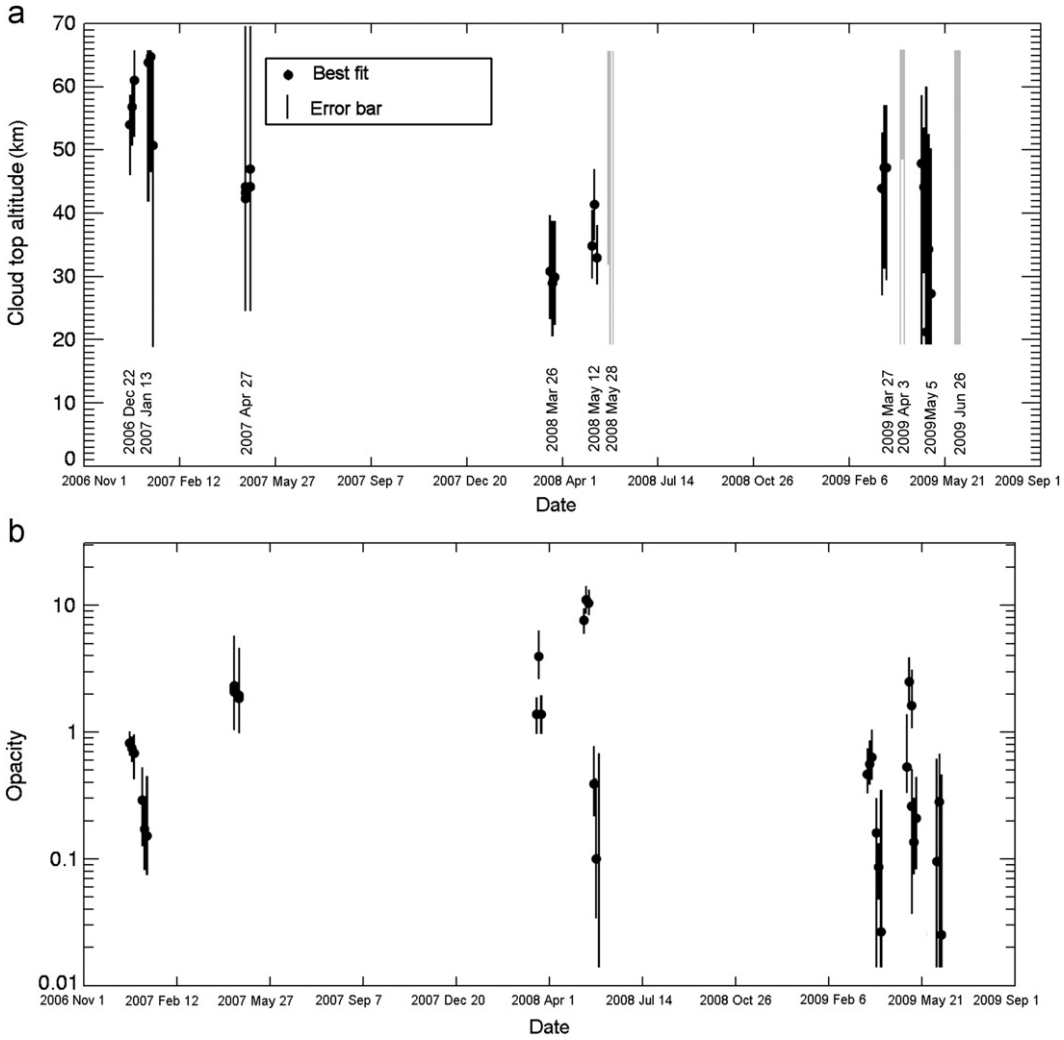

Fig. 4. (a) Cloud altitudes derived from the SPSDISORT radiative transfer model, computed on several pixels by flyby. The points correspond to the best fit, and the lines to errors bars for each point. The clouds are always found at the same altitude range, between 30 and 65 km. The modeling analysis did not allow to derive the altitude for the flybys T44, T52 and T56, probably due to a combined effect of the low spatial resolution and of the progressive decrease of the cloud thickness. (b) Cloud opacities derived from the SPSDISORT model.

the two types of clouds. We found no major altitude difference during T54 between the edge of the diffuse cloud and the more localized clouds near the pole.

Fig. 4b shows the retrieved cloud opacities, which vary from 0.03 for the cloud during T56 up to 10 for a pixel within the cloud during T43. These opacities can vary significantly from one pixel to the next in the same image. It should be noted that the retrieved opacities are not directly representative of the total cloud opacities. Indeed, we choose only pixels at the edge of the cloud system in order to compare them with a nearby reference pixel in the surrounding haze. This could introduce a bias. Moreover, the retrieved opacity also depends on the spatial resolution of the image since we may have pixels including unresolved areas not fully filled with clouds, which would decrease the estimated opacities. Finally, the derived opacity also depends on the intrinsic sharpness of the cloud system itself, which may give lower opacities at the edge than in the core of the cloud. These cautions about opacity retrievals could slightly affect the altitude retrieval and are taken into account in the error bars shown in Fig. 4.

5. Discussion and conclusion

A vast northern cloud was predicted by the Titan global climate model (GCM) developed at the Pierre-Simon Laplace Institute (IPSL-TGCM, Rannou et al., 2006), at the same location, altitude range and with the same latitudinal extension as the one observed by VIMS, at the precise location where all GCMs for Titan predict a descending branch of the pole-to-pole stratospheric cell (Tokano et al., 2001; Mitchell et al., 2006). Fig. 5 shows the predicted occurrence of clouds, averaged between 60°N and 90°N in latitude, and by time intervals of 10 Titan days (168 terrestrial days), derived from the IPSL-TGCM (Rannou et al., 2006). We plot in this figure three fractions of occupation by clouds having opacities ranging between 3 and 10, which are the typical modeled opacities considered for clouds seen from orbit. We see that the overall tendency corresponds to a decrease, which is expected to occur after 2005.

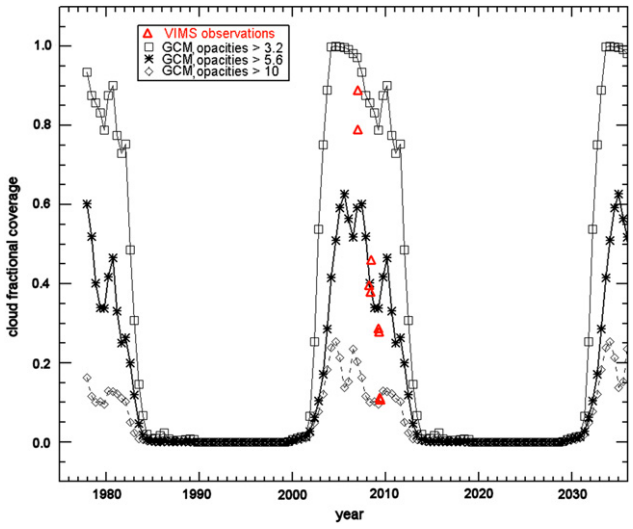

Fig. 5. Occurrence of clouds (fractional coverage between 0 and 1) averaged between latitudes 60°N and 90°N and by time intervals of 10 Titan days (168 terrestrial days), derived from the IPSL GCM (Rannou et al., 2006). The line with open squares corresponds to the fraction of occupation by clouds having opacities higher than 3.2. The line with stars corresponds to opacities greater than 5.6, and the dotted line with open diamonds corresponds to the fraction of occupation by clouds having opacities greater than 10. The percentage of spatial coverage of the clouds derived from the VIMS observations are indicated by the red triangles. The timing of the decrease in modeled cloud coverage is at first order consistent with the VIMS observations, and is directly connected to the seasonal change in circulation. (For interpretation of the references to color in this figure legend, the reader is referred to the web version of this article).

As a comparison, we have indicated on the same plot the percentage of spatial coverage of the clouds derived from the VIMS observations analyzed in this paper (red triangles). It corresponds to the number of pixels covered by clouds, which have been detected using the semi-automated algorithm of Rodriguez et al. (2009) applied on the whole images, divided by the total number of illuminated pixels at latitudes north of 60°N in the VIMS images shown in Fig. 2. The VIMS observations show that a significant decrease in cloud fractional coverage is indeed observed with time. The coverage was approximately 90% in December 2006, and drops down to less than 20% between April and June 2009. The timing and the intensity of the decrease predicted by the GCM are therefore to first order consistent with the VIMS observations (Fig. 5). We focus here on the overall tendency only (a nearly complete vanishing of the polar cloud when approaching the equinox). A detailed comparison of the model and the data would not be relevant since the two physical quantities are related, but not exactly similar. The timing of dissipation of this polar cloud, which is directly linked to the transport of material by the descending branch of the stratospheric circulation, illustrates the seasonal change in the circulation as the equinox approaches. The progressive disappearance of the north polar cloud is also important for designing forthcoming observations, when VIMS will have the first opportunities to operate at closest approach above the northern lakes.

At latitudes between $\pm 70^{\circ}$, average precipitation is not expected to exceed 1 cm per year, but poleward of $\pm 70^{\circ}$ it can reach 1 m per year in the summer hemisphere for methane, and 6 μm/year for ethane in the winter hemisphere (Rannou et al., 2006). A dedicated cloud backscatter RADAR observation (10 May 2007), similar to the ones used on Earth for meteorological surveys, was used to constrain the precipitation of material onto the surface at the north pole (Lorenz et al., 2008). The measurement showed that droplets were either extremely sparse or extremely small (or both), which ruled out the direct detection of rainfall at least at the location and time of this specific observation. The massive cloud system observed above the lakes could still play a role in the filling of the lakes during the winter season, despite the fact that lakes might by stable over more than one season (Lorenz et al., 2008, Aharonson et al., 2009). The reversal of the pole-to-pole circulation, which is predicted to occur at the equinox, should lead to significant changes in the cloud cover, and possibly the lake distribution, and will be monitored with the Cassini spacecraft up to 2017.

Acknowledgments

This work benefited from financial supports from the Centre National de la Recherche Scientifique, Institut National des Sciences de l'Univers, from the French Centre National d'Etudes Spatiales (CNES) and from the ANR (project ANR-07-BLAN-0127 exoclimat). The authors wish to thank E. Turtle and an anonymous reviewer for their thorough reviews.

References

Aharonson, O., Hayes, A.G., Lunine, J.I., Lorenz, R.D., Allison, M.D., Elachi, C., 2009. An asymmetric distribution of lakes on Titan as a possible consequence of orbital forcing. Nat. Geosci. Lett. 2, 851–854.

Barnes, J.W., et al., 2009. VIMS spectral mapping observations of Titan during the Cassini prime mission. Planet Space Sci. 57, 1950–1962.

Brown, M.E., Bouchez, A.H., Griffith, C.A., 2002. Direct detection of variable tropospheric clouds near Titan's south pole. Nature 420, 795–797.

Brown, M.E., Schaller, E.L., Roe, H.G., Chen, C., Roberts, J., Brown, R.H., Baines, K.H., Clark, R.N., 2009. Discovery of lake-effect clouds on Titan. Geophys. Res. Lett. 36, 1103.

Brown, R.H., et al., 2004. The Cassini visual and infrared mapping spectrometer (Vims) investigation. Space Sci. Rev. 115, 111–168.

Flasar, F.M., et al., 2005. Titan's atmospheric temperatures, winds, and composition. Science 308, 975–978.

Fulchignoni, M., et al., 2005. In situ measurements of the physical characteristics of Titan's environment. Nature 438 (7069), 785–791.

Griffith, C.A., Owen, T., Miller, G.A., Geballe, T., 1998. Transient clouds in Titan's lower atmosphere. Nature 395, 575–578.

Griffith, C.A., et al., 2005. The evolution of Titan's mid-latitude clouds. Science 310, 474–477.

Griffith, C.A., Penteado, P., Rannou, P., Brown, R., Boudon, V., Baines, K.H., Clark, R., Drossart, P., Buratti, B., Nicholson, P., McKay, C.P., Coustenis, A., Negrao, A., Jaumann, R., 2006. Evidence for a polar ethane cloud on Titan. Science 313, 1620–1622.

Griffith, A.A., Penteado, P., Rodriguez, S., Le Mouélic, S., Baines, K.H., Buratti, B., Clark, R.N., Nicholson, P.D., Jaumann, R., Sotin, C., 2009. Characterization of clouds in Titan's tropical atmosphere. ApJ Lett. 702, 105–109.

Hayes, A., Aharonson, O., Callahan, P., Elachi, C., Gim, Y., Kirk, R., Lewis, K., Lopes, R., Lorenz, R., Lunine, J., Mitchell, K., Mitri, G., Stofan, E., Wall, S., 2008. Hydrocarbon lakes on Titan: distribution and interaction with a porous regolith. Geophys. Res. Lett. 35, L09204. doi:10.1029/2008GL033409.

Irwin, P.G.J., Sihra, K., Bowles, N., Taylor, F.W., Calcutt, S.B., 2005. Methane absorption in the atmosphere of Jupiter from 1800 to 9500 cm^{-1} and implications for vertical cloud structure. Icarus 176 (2), 255–271.

Irwin, P.G.J., Sromovsky, L.A., Strong, E.K., Sihra, K., Teanby, N.A., Bowles, N., Calcutt, S.B., Remedios, J.J., 2006. Improved near-infrared methane band models and k-distribution parameters from 2000 to 9500 cm^{-1} and implications for interpretation of outer planet spectra. Icarus 181 (1), 309–319.

Jennings, D.E., et al., 2009. Titan's Surface Brightness Temperatures. ApJ Lett. 691, 103–105.

Karkoschka, E., Tomasko, M.G., 2010. Methane absorption coefficients for the jovian planets from laboratory, Huygens, and HST data. Icarus 205 (2), 674–694.

Lavvas, P.P., Coustenis, A., Vardavas, I.M., 2008. Coupling photochemistry with haze formation in Titan's atmosphere, Part II: results and validation with Cassini/Huygens data. Planet Space Sci. 56, 67–99.

Lorenz, R.D., West, R.D., Johnson, W.T.K., 2008. Cassini RADAR constraint on Titan's winter polar precipitation. Icarus 195, 812–816.

Mayer, B., Kylling, A., 2005. Technical note: the libRadtran software package for radiative transfer calculations—description and examples of use. Atmos. Chem. Phys. Discuss. 5, 1855–1877.

Mitchell, J.L., Pierrehumbert, R.T., Frierson, D.M.W., Caballero, R., 2006. The dynamics behind Titan's methane clouds. Proc. Natl. Acad. Sci. USA 103, 18421–18426.

Niemann, H.B., Atreya, S.K., Bauer, S.J., Carignan, G.R., Demick, J.E., Frost, R.L., Gautier, D., Haberman, J.A., Harpold, D.N., Hunten, D.M., Israel, G., Lunine, J.I., Kasprzak, S.H., Owen, T.C., Paulkovich, M., Raulin, F., Raaen, E., Way, S.H., 2005. The abundances of constituents of Titan's atmosphere from the GCMS instrument on the Huygens probe. Nature 438 (7069), 779–784.

Porco, C.C., et al., 2005. Imaging of Titan from the Cassini spacecraft. Nature 434, 159–168.

Rannou, P., Lebonnois, S., Hourdin, F., Luz, D., 2005. Titan atmosphere database. Adv. Space Res. 36 (11), 2194–2198.

Rannou, P., Montmessin, F., Hourdin, F., Lebonnois, S., 2006. The latitudinal distribution of clouds on Titan. Science 311, 201–205.

Rannou, P., Cours, T., Le Mouélic, S., Rodriguez, S., Sotin, C., Drossart, P., Brown, R., Clark, R.N., Barnes, J.W., Baines, K.H., Buratti, B.J., Nicholson, P.D., 2010. Titan haze distribution and optical properties retrieved from recent observations. Icarus 208, 850–867.

Rodriguez, S., Le Mouélic, S., Rannou, P., Tobie, G., Baines, K.H., Barnes, J.W., Griffith, C.A., Hirtzig, M., Pitman, K.M., Sotin, C., Brown, R.H., Buratti, B.J., Clark, R.N., Nicholson, P.D., 2009. Global circulation as the main source of cloud activity on Titan. Nature 459, 678–682.

Roe, H.G., de Pater, I., Macintosh, B.A., McKay, C.P., 2002. Titan's clouds from Gemini and Keck adaptive optics imaging. ApJ 581, 1399–1406.

Roe, H.G., Bouchez, A.H., Trujillo, C.A., Schaller, E.L., Brown, M.E., 2005. Discovery of temperate latitude clouds on Titan. ApJ 618, 49–52.

Schaller, E.L., Brown, M.E., Roe, H.G., Bouchez, A.H., Trujillo, C.A., 2006. Dissipation of Titan's south polar clouds. Icarus 184, 517–523.

Schaller, E.L., Roe, H.G., Schneider, T., Brown, M.E., 2009. Storms in the tropics of Titan. Nature 460, 873–875.

Sromovsky, L.A., Suomi, V.E., Pollack, J.B., Kraus, R.J., Limaye, S.S., Owen, T., Revercomb, H.E., Sagan, C., 1981. Implication of Titan's north–south brightness asymmetry. Nature 292, 698.

Stofan, E.R., et al., 2007. The lakes of Titan. Nature 445, 61–64.

Tokano, T., Neubauer, F.M., Laube, M., McKay, C.P., 2001. Three-dimensional modeling of the tropospheric methane cycle on Titan. Icarus 153, 130–147.

Tomasko, M.G., Bézard, B., Doose, L., Engel, S., Karkoschka, E., 2008. Measurements of methane absorption by the descent imager/spectral radiometer (DISR) during its descent through Titan's atmosphere. Planet Space Sci. 56, 624–647.

Tomasko, M.G., Archinal, B., Becker, T., Bézard, B., Bushroe, M., Combes, M., Cook, D., Coustenis, A., DeBergh, C., Dafoe, L.E., Doose, L., Douté, S., Eibl, A., Engel, S., Gliem, F., Grieger, B., Holso, K., Howington-Kraus, E., Karboschka, E., Keller, H.U., Kirk, R., Kramm, R., Küppers, M., Lanagan, P., Lellouche, E., Lemmon, M., Lunine, J., McFarlane, E., Moores, J., Prout, G.M., Rizk, B., Rosiek, M., Rueffer, P., Schröder, S.M., Schmitt, B., See, C., Smith, P., Soderblom, L., Thomas, N., West, R., 2005. Rain, wind and haze during the Huygens probe's descent to Titan's surface. Nature 438, 765–778.

Turtle, E.P., Perry, J.E., McEwen, A.S., DelGenio, A.D., Barbara, J., West, R.A., Dawson, D.D., Porco, C.C., 2009. Cassini imaging of Titan's high-latitude lakes, clouds, and south-polar surface changes. Geophys. Res. Lett. 36, L02204.

Turtle, E., et al., 2011. Seasonal changes in Titan's meteorology. Geophys. Res. Lett. 38, L03203. doi:10.1029/2010GL046266.